ANALYSIS OF AVIRIS DATA FROM LEO-15 USING *TAFKAA* ATMOSPHERIC CORRECTION

Marcos J. Montes,[*] Bo-Cai Gao,[†] Curtiss O. Davis,[‡] and Mark Moline[§]

1 INTRODUCTION

We previously developed an algorithm named Tafkaa for atmospheric correction of remote sensing ocean color data from aircraft and satellite platforms. The algorithm allows quick atmospheric correction of hyperspectral data using lookup tables generated with a modified version of Ahmad & Fraser's vector radiative transfer code. During the past few years we have extended the capabilities of the code. Current modifications include the ability to account for within scene variation in solar geometry (important for very long scenes) and view geometries (important for wide fields of view). Additionally, versions of Tafkaa have been made for a variety of multi-spectral sensors, including SeaWiFS and MODIS. In this proceeding we present some initial results of atmospheric correction of AVIRIS data from the 2001 July Hyperspectral Coastal Ocean Dynamics Experiment (HyCODE) at LEO-15.

2 BACKGROUND

Over the past two decades, atmospheric correction algorithms for application to case 1 waters (i.e., clear, deep ocean waters) have been developed by Howard Gordon's research group at the University of Miami, Florida. The complexity of these algorithms has increased greatly with time- from the early single scattering algorithm used for CZCS (Gordon, 1978) to the present more complete multiple scattering algorithm for SeaWiFS (Gordon & Wang, 1994). For the operational SeaWiFS algorithm, a simplified two-layer atmosphere system, i.e., aerosols being confined in the bottom boundary layer and atmospheric gaseous molecules being located in another layer above the aerosol layer, is assumed. An aerosol model and an aerosol optical depth are derived from channels located centered at 0.76 and 0.87 μm by assuming water-leaving radiances to be zero in that spectral range. A sophisticated lookup table procedure is used for the aerosol retrievals. The atmospheric path radiances in the visible are predicted based on the derived aerosol information. The difference between the measured radiances above the atmosphere-ocean system and the predicted path-radiance is the water-leaving radiance transmitted to the top of the atmosphere.

However, this approach does not work for some ocean environments. Over a bright sand bottom, a turbid coastal environment, or a coccolithophore bloom the water-leaving radiances in the 0.66-0.87 μm range are typically not close to zero. In the former case, reflectance by bright ocean bottoms in optically shallow water causes much more water-leaving radiance at these wavelengths than is measured in open oceans with similar water types. In the latter cases, this is due to scattering by suspended materials. Under these conditions, the channels in this spectral region have very limited use for the retrieval of information on atmospheric aerosols. The algorithms of Gordon (1997) and Fraser et al. (1997) derive aerosol information from channels in the 0.66-0.87 μm spectral range. These algorithms cannot be easily adapted for the retrieval of water-leaving radiances over coastal waters. In view of this situation, we have designed a different retrieving algorithm that can use channels in longer wavelengths, in addition to these channels, to derive aerosol information.

Since the liquid water absorption increases rapidly as a function of wavelength (Wieliczka et al., 1989), one can assume that the water-leaving radiance is zero at long enough wavelengths, even in turbid waters or over bright, shallow bottoms. In this case, one can use two or more of the atmospheric transmission window regions near 0.865, 1.04, 1.24, 1.64, and/or 2.25 μm in order to determine the aerosol type and optical depth. Our Tafkaa aerosol lookup tables include all of those wavelengths, in addition to several in the VNIR portion of the spectrum. The tables were calculated with Ahmad & Fraser's (1982) radiative transfer code that includes all orders of scattering, and components of polarization. The lower boundary condition is a rough ocean surface with capillary wave distribution as described by Cox & Munk (1954), as well as the effects of foam. The tables were calculated at 14 wavelengths and 3 wind speeds. There are 10 aerosol optical depths, 5 overall aerosol models, each of which has 5 size distributions (i.e., relative humidities). The geometrical grids have 9 solar zenith angles (θ_0), 17 view zenith angles (θ), and 17 relative azimuth angles ($\Delta\phi$). The calculations were output at 9 sensor altitudes, and all the calculations

[*] Remote Sensing Division, Code 7232, Naval Research Laboratory, Washington, D.C. 20375 (corresponding author: Marcos.Montes@NRL.Navy.mil)
[†] Remote Sensing Division, Code 7232, Naval Research Laboratory, Washington, D.C. 20375
[‡] Remote Sensing Division, Code 7203, Naval Research Laboratory, Washington, D.C. 20375
[§] Biological Science Dept., California Polytechnic State University, San Luis Obispo, California 93407.

assume a surface at sea-level. A thorough description of our algorithm may be found in Gao et al. (2000), and modifications are described in Montes et al. (2001) and Montes et al. (2003).

3 OVERVIEW OF THE LEO-15 SITE

The study site was the area in and around the Long-term Ecosystem Observatory in 15 m of water (i.e., LEO-15). This site is in the middle of the Middle-Atlantic Bight, off the coast of New Jersey, as shown in Fig. 1. The principal moorings are in about 15 m of water, and are about 22 km northeast of Atlantic City, New Jersey. The presence of the moorings and other underwater instrumentation led to LEO-15 becoming one of the diagnostic data sites used by the SIMBIOS project. Much of the of the area is very shallow, with depths of $z < 10$ m even a few kilometers offshore, as can be seen in Fig. 1b. The river outflow, tidal action, and the shallow water lead to the ubiquitous presence of suspended sediments throughout this area. Furthermore, high nutrient concentrations from river outflow and frequent episodic upwelling in the shallow system, allows for the rapid growth and accumulation of phytoplankton in this area.

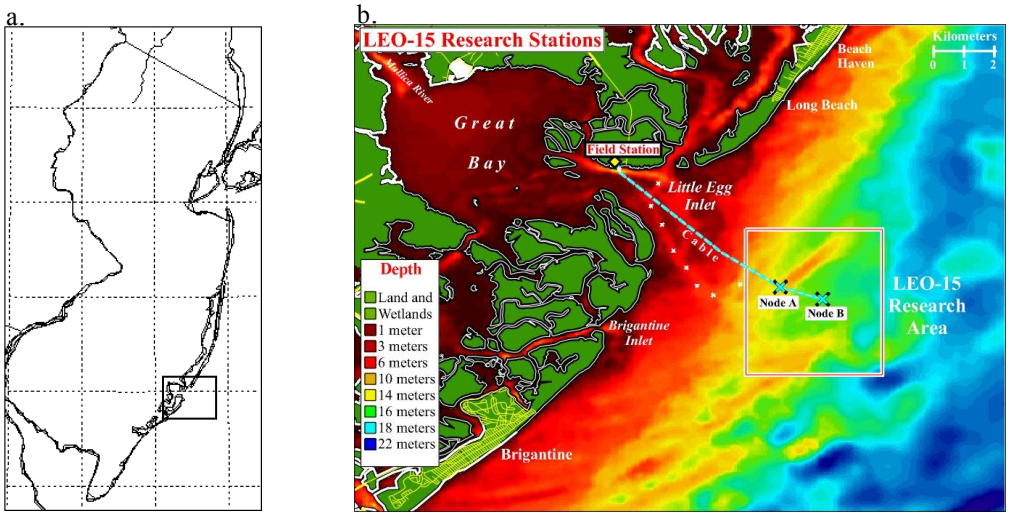

Figure 1. a.) A map of New Jersey, with an inset showing the approximate location of the map to the right. b.) A bathymetric map showing the location of the LEO-15 research area in relation to various geographic locations. (This image is courtesy of the Coastal Ocean Observation Lab, Institute of Marine and Coastal Sciences, Rutgers University.)

In July and August 2001, as a part of the HyCODE, a multi-institution collaboration measured ocean properties with a number of instruments deployed in the space, air, on the water's surface, and in the water in and around LEO-15. On July 31, 2001, hyperspectral and multispectral observations were obtained, as well as measurements from 5 research vessels and a number of in-situ autonomous systems. Imaging data at varying GSD was obtained from the multi-spectral sensors SeaWiFS and MODIS (~1 km GSD), as well as the hyperspectral instruments AVIRIS (~17 m GSD), PHILLS-2 (~9 m GSD), and PHILLS-1 (~2 m GSD). The various in-water and shipboard measurements provide us with the tools to perform closure experiments. In-water depth profiles of absorption and scattering allow us to compute forward models to compare with the water-leaving radiance measurements derived with Tafkaa, as well as allowing us to compare with shipboard measurements of remote-sensing reflectance.

The MODIS and SeaWiFS apparent reflectance images (Fig. 2) present a snapshot overview of the region around LEO-15 at ~16:24 and 18:00 GMT (i.e., about 40 minutes before and 55 minutes after local solar noon at the LEO-15 site), respectively. For this subsection of the MODIS image, geometries were $21.8° < \theta_0 < 23.8°$ and $33.3° < \theta < 42.3°$. Likewise, for the subsection of the SeaWiFS image, geometries were $23.4° < \theta_0 < 25.6°$ and $49.1° < \theta < 55.4°$. Both land (at the left) and clouds (lower right corner) have been masked in these images.

The July 31, 2001, AVIRIS apparent reflectance mosaic shown in Fig. 3 covers the entire region of Fig. 1b, but makes up only a small portion of the images in Fig. 2. The AVIRIS data consists of six runs during the local morning, i.e., from 13:47 GMT to 14:49 GMT (f010731t01p03_r0[2-7]). During that time, the solar zenith angle varied from 46.7° to 36.2°. For the mostly level flight of the ER-2, the AVIRIS images had the typical ~30° wide, nadir-oriented field of view. Figure 2 shows five of the six runs; run r03 evenly overlaps runs r02 & r04, and is omitted from the mosaic. The start and stop times, as well as the values for the solar zenith angle, solar azimuth angle, and heading at the center of the flight lines are listed in Table 1. The AVIRIS flight lines were planned to

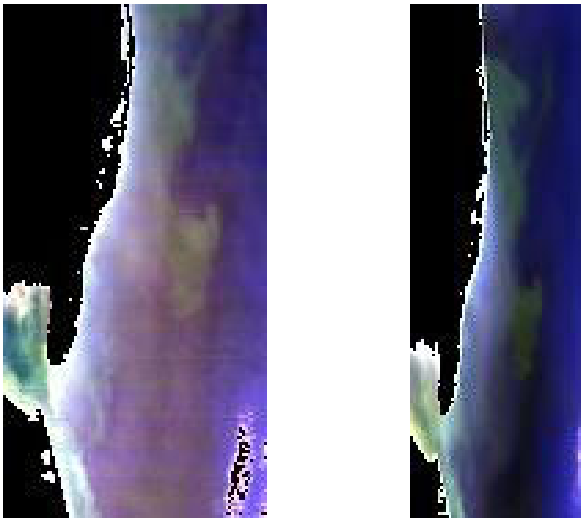

Figure 2: MODIS (left) and SeaWiFS (right) images of similar areas of the New Jersey coast around the LEO-15 site. Both images show observed reflectance, i.e., $\pi L_{obs}/(\mu_0 E_0)$ from 2001 July 31. The MODIS image (channels 13, 12, and 9) was obtained about 16:24 GMT, and the SeaWiFS image (channels 6, 5, and 2) was obtained about 18:00 GMT. Delaware Bay and Cape May, N.J., are easily recognized in the mid-lower left portion of each image. Neither image has been geometrically corrected.

overlap at the edges, to be mostly parallel, and to fly into or out of the sun to reduce the specular reflection of the direct solar beam from the ocean surface. Additional AVIRIS flights were obtained beginning 24 hours later on August 1, 2001 (f010801t01p03_r0[2-7]), along essentially the same flight paths. The August 1, 2001, data set has some offshore clouds in it, and was not studied for this paper. This area was also previously imaged in 1998 using AVIRIS (f980712t01p02_r03) along a flight line with very similar parameters to f010731t01p03_r03. A close examination of the AVIRIS mosaic shows that the features on the land do not quite overlap in neighboring runs. The georectification will be improved once we obtain the 10Hz navigation files for each of the flight lines, and will be necessary for some comparisons with data obtained from instruments in the ocean.

In comparison with Fig. 2, the MODIS and SeaWiFS images present a snapshot of the whole region, and allow for very uniform lighting conditions across the image since θ_0 and θ change very little across these sub-images, and even less over the smaller area spanned by the AVIRIS mosaics. In the AVIRIS mosaic one can easily see the lighting variations on the different runs, and even cross-track lighting variations within a run. On the other hand, the much smaller GSD of the AVIRIS image allows us to see many features in the coastal waters, estuaries, and bays that are not resolved in the MODIS and SeaWiFS images. The hyperspectral nature of AVIRIS allows researchers to determine aerosol parameters, as well as the promise of being able to derive in-water parameters such as bottom classification and bathymetry (Mobley et al. 2002; Lee et al. 2001), work that typically cannot be done with large-GSD multispectral imagers.

4 ATMOSPHERIC CORRECTION OF THE AVIRIS SCENES

We are in the process of correcting the AVIRIS scenes for atmospheric effects. For this work, we are using the latest version of Tafkaa, which allows for more exact corrections of solar and view geometry, as described in Montes et al. (2003). We assumed the pixel-to-pixel angular separation was 0.8715 milliradians, and that AVIRIS was mounted so that the center of the scan was nadir viewing. There are small deviations in roll and pitch that affect the pointing of the sensor (and therefore the view geometry); these have been ignored at this point. The solar zenith angle was computed for the center of each 614 sample line of data using the 1 Hz updated values of the latitude, longitude, and time, and assuming a flat surface, so the solar zenith angles change only every 12 lines, which is sufficient for a scene this size.

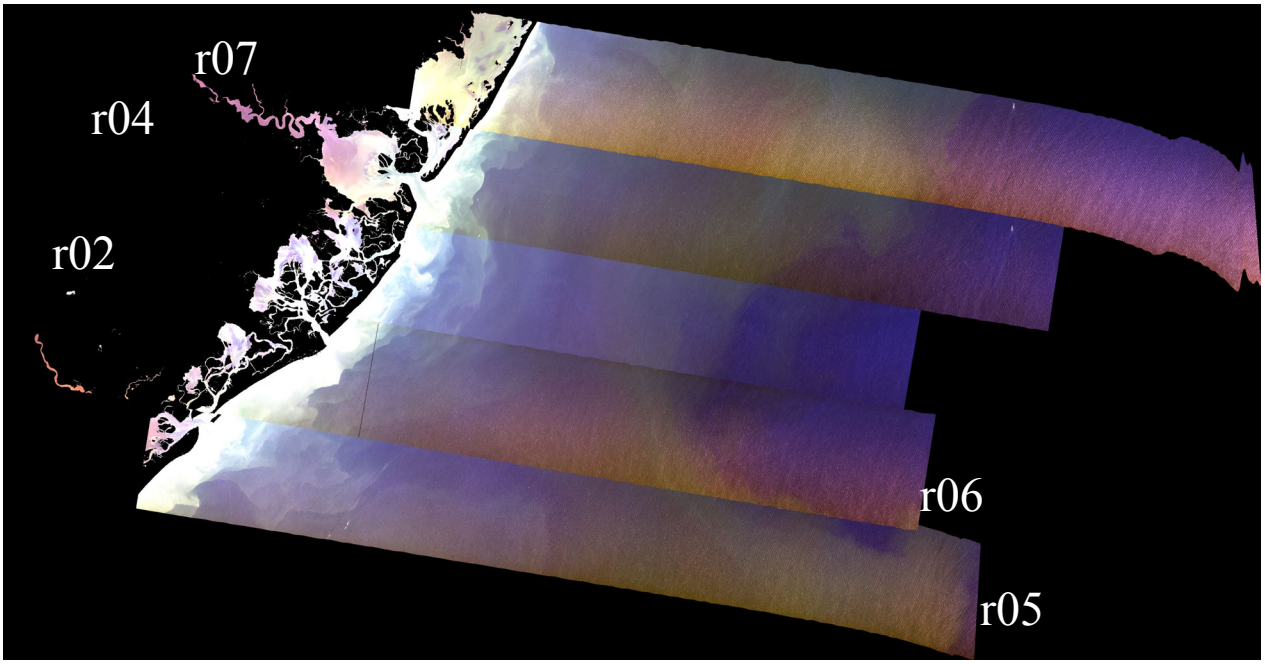

Figure 3. A mosaic of the AVIRIS data from 2001 July 31, excluding run r03 since it overlaps parts of runs r02 and r04. The times, headings, and solar geometry for each flight line are listed in Table.1. This RGB is made from apparent reflectance [$\rho_a = \pi L_{obs} / (\mu_0 E_0)$] maps at 664, 548, and 442 nm. The colors have been stretched to emphasize the features in the deep water. The georectification for this image used the AVIRIS provided *.igm files.

Table 1. The times and geometric information for the AVIRIS runs over the LEO-15 site on 2001 July 31. θ_0 is the mean solar zenith angle, ϕ_0 is the mean solar azimuth angle, and Θ_h is the mean heading for each run.

	GMT		Degrees		
Run	Start	End	θ_0	ϕ_0	Θ_h
r02	13:46:49	13:52:14	46.	102.7	100
r03	13:58:16	14:04:20	44.	105.3	280
r04	14:09:21	14:16:54	42.	107.7	99
r05	14:20:26	14:26:32	40.	109.8	279
r06	14:31:01	14:37:58	38.	112.5	100
r07	14:43:17	14:49:24	36.	116.3	279

As mentioned previously, we must assume that $L_w = 0$ for certain wavelengths in order to derive the aerosol parameters from the data. False-color RGB images constructed from combinations of the aforementioned channels can assist in the choice. Ideally, we choose 3 or 4 channels in which there is no variation in radiance that can be associated with in-water features, as well as being the bluest channels available (since the solar irradiance, and hence the measured signal, decreases as the radiance increases in the NIR and SWIR).

For this example, we show the results from run 4, scene 5 (f010731t01p03_r04_s05), a region associated with the fronts east-southeast of Great Bay in run 04 (see Figs. 1 & 3). The images both before and after atmospheric correction are shown in Fig. 4. The ER-2 was flying from the top of the image to the bottom of the image, and the sun was about 8° to the right of the plane (i.e., on the left side of the image). In both images, it is easy to see a wave

pattern due to swells, and it is more prevalent on the sunward side of the image. In this example, we use a version of Tafkaa that determines aerosol properties at each pixel, using the NIR/SWIR windows. The output image is on the left side of Fig. 4., output spectra from the labeled areas are shown in Fig. 5. The output image shows wave features that are more prominent than in the input scene. The reason for this is quite simple: the brighter swells are interpreted as being a different aerosol, usually one that is more optically thick. Subtracting this (wrong) aerosol from the observed spectrum give a result where because of the large swell pattern, much of the output spectrum is negative. In this case, the best approach is to either input the aerosol type from measurements made at the time of the overflight, or to determine the aerosol parameters from select pixels in clear water that avoids the swells. Either approach may be used with Tafkaa.

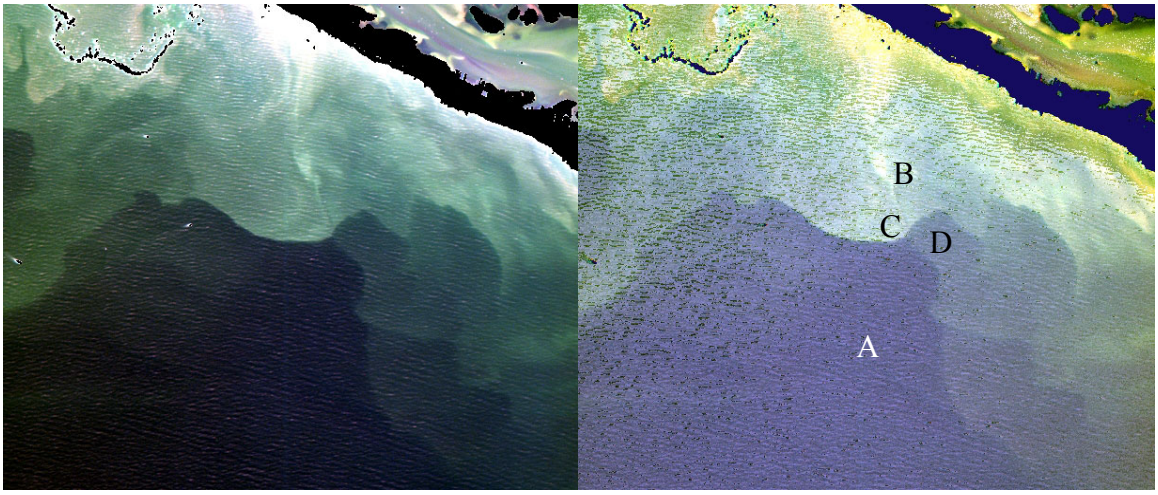

Figure 4. Apparent reflectance image of non-georectified run04, scene05 before atmospheric correction (left), and the same image after atmospheric correction (right). In both cases, the bands used to construct the RGB image are the same as in Fig. 2. The land has been masked in each image. Slopes of swells are obvious in both the uncorrected and corrected images, and are discussed in the text.

Having said that, there are many regions that return quite reasonable water-leaving reflectance (ρ_w) spectra, as shown in Fig. 5. The chlorophyll fluorescence peak is apparent at about 0.685 μm in all the spectra, indicating a high level of phytoplankton. The brightest spectrum (B) shows a small feature at about 0.810 μm that is due to a local minimum in the liquid water absorption spectrum and therefore indicates the presence of very shallow water or extremely high levels of suspended sediments in the top few meters of water.

5 DISCUSSION

Atmospheric correction of aquatic scenes is quite challenging since we must subtract most of the observed signal in order to obtain the water-leaving reflectance. Indeed, in the NIR/SWIR spectral regions we subtract *all* of the observed radiance since we assume the observed signal in this portion of the spectrum is entirely due to the atmosphere and specular reflection due to skylight. Stringent requirements for spectral and radiance calibration become very important in this environment. At such low light levels we see artifacts from the sensor, as well as artifacts in the method (i.e., improperly corrected swells). Research is ongoing in determining the best treatment of swells. Masking swells is an option, but might remove too many pixels from some scenes. Applying a uniform aerosol over the scene avoids selection of the wrong aerosols over swells, but it does not correctly account for the varying specular reflection over the swell's slopes.

6 ACKNOWLEDGEMENTS

The authors gratefully acknowledge the support of the U.S. Office of Naval Research for this research. M. Moline gratefully acknowledges the support of NASA (NAG5-8674).

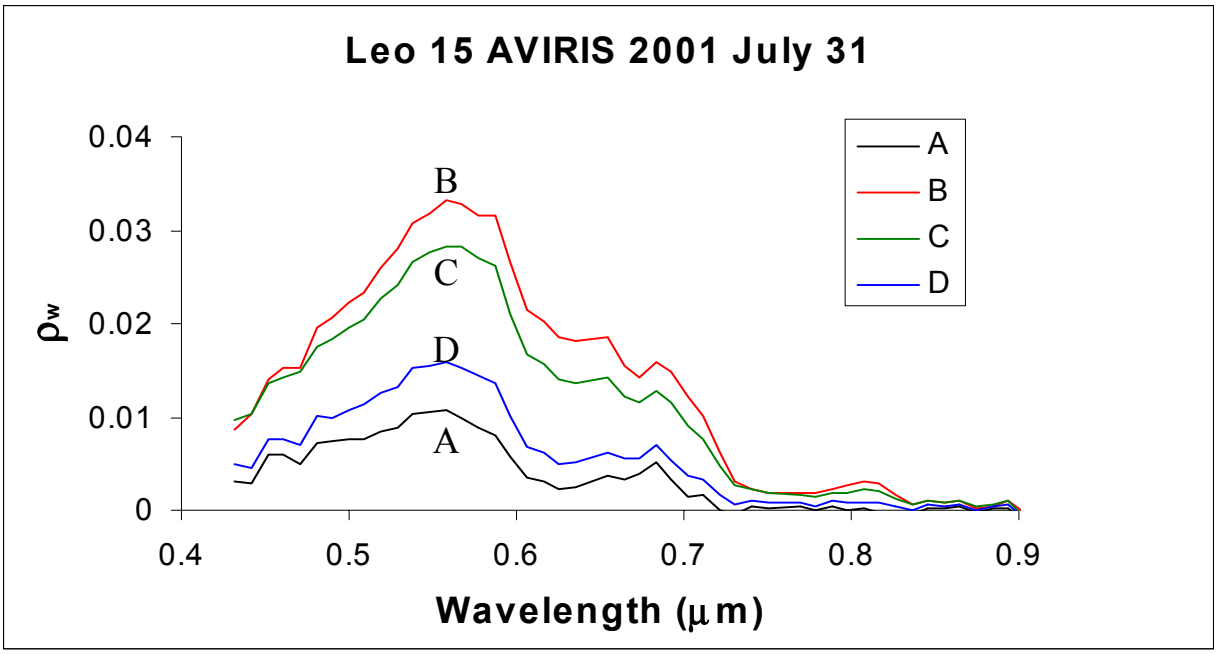

Figure 5. Atmospherically corrected water leaving reflectance (ρ_w) spectra from the labeled regions in Fig. 4.

7 REFERENCES

Ahmad, Z. and R. S. Fraser, 1982, "An iterative radiative transfer code for ocean-atmosphere systems," *J. Atmos. Sci.*, 39, 656-665.

Cox, C., and W. Munk, 1954, "Statistics of the sea surface derived from sun glitter," *J.Mar. Res.*, 14, 63-78.

Fraser, R. S., S. Matoo, E.-N. Yeh, and C. R. McClain, 1997, "Algorithm for atmospheric and glint corrections of satellite measurements," *J. Geophys. Res.*, 102, 17107-17118.

Gao, B.-C., M. J. Montes, Z. Ahmad, and C. O. Davis, 2000, "Atmospheric correction algorithm for hyperspectral remote sensing of ocean color from space", *Appl. Opt.*, 39, 887-896.

Gordon, H. R., 1978, "Removal of atmospheric effects from satellite imagery of the oceans," *Appl. Opt.*, 17, 1631-1636.

Gordon, H. R., 1997, "Atmospheric correction of ocean color imagery in the Earth Observing System era," *J. Geophys. Res.*, 102, 17081-17106.

Gordon, H. R. and M. Wang, 1994, "Retrieval of water leaving radiance and aerosol optical thickness over the oceans with SeaWiFS: A preliminary algorithm," *Appl. Opt.*, 33, 443-452.

Lee, Z., K. L. Carder, R. F. Chen, and T. G. Peacock, 2001, "Properties of the water column and bottom derived from Airborne Visible Infrared Imaging Spectrometer (AVIRIS) data," *J. Geophys. Res.*, 106, No. C6, 11639-11651.

Mobley, C. D., L. K. Sundman, C. O. Davis, M. J. Montes, W. P. Bissett, 2002, "A Look-Up-Table Approach to Inverting Remotely Sensed Ocean Color Data," on the *Ocean Optics XVI* compact disc.

Montes, M. J., B.-C. Gao, and C. O. Davis, 2001, "A new algorithm for atmospheric correction of hyperspectral remote sensing data," in *Geo-Spatial Image and Data Exploitation II*, W. E. Roper, ed., *Proc. SPIE*, 4383, 23-30.

Montes, M. J., B.-C. Gao, and C. O. Davis, 2003, "Tafkaa atmospheric correction of hyperspectral data," in *Imaging Spectrometry IX*, S. S. Shen and P. E. Lewis, eds., *Proc. SPIE*, 5159, in press.

Wieliczka, D. M., S.-S. Weng, and M. R. Querry, 1989, "Wedge shaped cell for highly absorbent liquids: Infrared optical constants of water", *Appl. Opt.*, 28, 1714-1719.